

# Axial dispersion and mixing of coolant gas within a separate-effect prismatic modular reactor

Ibrahim A. Said<sup>1,2</sup>, Mahmoud M. Taha<sup>1,2</sup>, Vineet Alexander<sup>1</sup>, Shoaib Usman<sup>3</sup>, Muthanna H. Al-Dahhan<sup>3</sup>

<sup>1</sup> *Multiphase Reactors Engineering and Applications Laboratory (mReal), Chemical and Biochemical Engineering Department, Missouri University of Science and Technology, Rolla, MO, 65409, USA*

<sup>2</sup> *Chemical Engineering Department, Faculty of Engineering, Alexandria University, Egypt*

<sup>3</sup> *Mining and Nuclear Engineering Department, Missouri University of Science and Technology, Rolla, MO, 65409-0170, USA*

Corresponding author: *Muthanna H. Al-Dahhan (aldahhanm@mst.edu)*

---

**Academic editor:** *Yury Korovin* ♦ **Received** 10 June 2018 ♦ **Accepted** 23 October 2018 ♦ **Published** 7 December 2018

---

**Citation:** Said IA, Taha MM, Alexander V, Usman S, Al-Dahhan MH (2018) Axial dispersion and mixing of coolant gas within a separate-effect prismatic modular reactor. *Nuclear Energy and Technology* 4(3): 167–178. <https://doi.org/10.3897/nucet.4.27346>

---

## Abstract

Multiphase Reactors Engineering and Applications Laboratory performed gas phase dispersion experiments in a separate-effect cold-flow experimental setup for coolant flow within heated channels of the prismatic modular reactor under accident scenario using gaseous tracer technique. The separate-effect experimental setup was designed on light of local velocity measurements obtained by using hot wire anemometry. The measurements consist of pulse-response of gas tracer that is flowing through the mimicked riser channel using air as a carrier. The dispersion of the gas phase within the separate-effect riser channel was described using one-dimensional axial dispersion model. The axial dispersion coefficient and Peclet number of the coolant gas phase and their residence time distribution within were measured. Effect of heating intensities in terms of heat fluxes on the coolant gas dispersion along riser channels were mimicked in the current study by a certain range of volumetric air flow rate ranging from 0.0015 to 0.0034 m<sup>3</sup>/s which corresponding to heating intensity range from 200 to 1400 W/m<sup>2</sup>. Results confirm a reduction in the response curve spreads is achieved by increasing the volumetric air velocity (representing heating intensity). Also, the results reveal a reduction in values of axial dispersion coefficient with increasing the air volumetric flow rate.

---

## Keywords

Prismatic modular reactor; gaseous tracer technique; axial dispersion coefficient; Peclet number

---

## Introduction

The prismatic modular reactor (PMR) is one of the next generation nuclear plants (NGNPs). One of the prismatic modular reactor (PMR) advantages is its capability to passively remove the decay heat from the reactor core through natural circulation under the loss of flow accidents (LOFA) scenario (Tung et al. 2013). In the

scenario of the loss of flow accident (LOFA), the natural circulation, due to large temperature variations and consequently density differences, is initiated to remove the decay heat from the reactor core. Furthermore, during the LOFA event, the direction of the coolant flows within the reactor core is reversed. There are two different possibilities for the flow direction within the of the coolant flow channels due to large densities variations of the coolant.

For the heated portions of the reactor core, the gas coolant flows upward, while in the relatively cooled portions (lower temperature) the gas coolant flows downward establishing the natural circulation. The gas coolant channels with downward flow act as downcomer channels, while the coolant channels with upward flow act as riser channels. A description and more details regarding the prismatic modular reactor under accident scenario is given by Said et al. (Abdallah 2017, Said et al. 2018, Said et al. 2018). The efficiency of the natural circulation as a safety feature of the prismatic modular reactor is dependent upon how the gas coolant removes the decay heat from the reactor core. Therefore, to reliably simulate the thermal hydraulic phenomena within the reactor core, the gas-coolant heat transfer and dynamics need to be characterized by a representative geometry. In the open literature, there are few studies performed on the flow field in the prismatic modular reactor under the natural circulation using computational fluid dynamics (CFD) to address the thermal performance of PMR after LOFA under natural using different turbulence models as well as heat transfer mechanisms (Haque et al. 2006, Simoneau et al. 2007, Tung and Johnson 2011, Aldridge 2013, Tung et al. 2013, Tung et al. 2014, Tung et al. 2016). Furthermore, there are unique experimental studies that were performed in the Multiphase Reactors Engineering and Applications Laboratory (mReal) at Missouri S&T, Rolla that are directed to understand the heat transfer and coolant dynamics within a dual-channel circulation loop under high pressure and temperature (Moharam 2017, Said et al. 2017, Al-Shahri et al. 2018, Taha et al. 2018a, Taha et al. 2018b, Said et al. 2018a, Said et al. 2018b). Said et al. at mReal research team implemented sophisticated measurement techniques, including hot wire anemometry, radial temperature T-thermocouple adjuster, and heat transfer coefficient probe to experimentally measure and analysis local coolant velocities, temperature fields (coolant and inner wall temperatures), and local heat transfer coefficients along the flow channels under different operating conditions. To the authors acknowledge, there are no reported studies in the open literature related to quantifying and understanding the gas coolant dispersion along the flow channels of the prismatic modular reactor (PMR) under an accident or normal scenarios. The only available experimental studies in the open literature are oriented to empty tubes under different operating and design conditions (Wen and Fan 1975). Unfortunately, these studies are carried out in non-representative geometries and operating conditions that cannot be extended to the prismatic modular reactor under LOFA scenario. Hence, extensive quantification and analysis are carried out at mReal using advanced sophisticated gaseous tracer technique, for the first time, to advance the knowledge of the gas coolant mixing and dispersion occurring in the flow channels of the prismatic modular reactor under accident scenario. Implementation of the gas dispersion and mixing measurements using the gaseous tracer technique within the dual-channel cir-

ulation loop of Said et al. at mReal (Said et al. 2018a, Said et al. 2018b) is technically challenging and will not produce reliable benchmark data due to temperature limitations and other difficulties as discussed in the next section of the *experimental work*. Hence, the measured local gas coolant velocities along the riser channel of the dual-channel circulation loop under different heating intensities (200 to 1400 W/m<sup>2</sup>) (Moharam 2017) were used to design and develop the current cold-flow separate-effect test section which mimics the riser channel of the dual-channel circulation loop at mReal under cold flow conditions. This is executed by matching the local gas coolant velocities between the riser channel in the dual-channel circulation loop, which is designed at mReal with reference to high-temperature test facility at Oregon State University (Castañeda 2014, Said et al. 2017) and the current separate-effect test section for atmospheric air condition. This is achieved by adjusting the input volumetric air flow rate to the test section to get similarity in terms of local air velocity between the separate effect test section and the dual-channel circulation loop. The effect of the heating intensity, ranging from 200 to 1400 W/m<sup>2</sup>, in terms of adjusted volumetric air flow rate, ranging from 0.0015 to 0.0034 m<sup>3</sup>/s, on the axial dispersion coefficients of the coolant was investigated along the riser channel within a cold-flow separate-effect facility. The deviation of the coolant flow from the plug flow condition along the riser channel is described using the one-dimensional axial dispersion model (1D-ADM). In the open literature, almost no experimental studies of gas phase dispersion of the coolant in a representative geometry of the PMR reactor were found. Thus, the current study provides high temporal resolutions and spatial benchmarking data in terms of axial dispersion coefficients that can be used as an input for the mass transfer correlations of the coolant in the PMR for safe, efficient design, and operation of the PMR under accident scenarios.

## Experimental work

Multiphase Reactors Engineering and Applications Laboratory (mReal) research team at Missouri S&T designed and constructed a high pressure and temperature dual-channel facility, mimicking prismatic modular reactor (PMR), for natural circulation passive safety system heat transfer and gas dynamics investigations (Said et al. 2017). Implementation of the gas dispersion measurements using the gaseous tracer technique in this facility is technically challenging and will not produce reliable measurements in terms of residence time distributions (RTD). These difficulties arise from the following: 1) temperature limitations (the thermal conductivity detector component of the gaseous tracer technique cannot withstand temperature exceeds 40 °C), 2) accumulation of the gas tracer within the dual-channel at mReal (the dual-channel facility is a closed system under high pres-

sure and temperature, and there is an opportunity for the accumulation of the tracer that will affect the measured signals repeatability), and 3) gas dispersion instrumentation vacuum pumping components would affect naturally-driven flow within the dual-channel facility. Hence, a separate effect cold-flow convergent channel was designed and developed for gas dispersion investigations mimicking naturally-driven upward flow within the riser coolant channel of the dual-channel facility. Therefore, this separate-effects convergent channel was designed with the guidance of local velocity measurements of the dual-channel facility operated under different heating intensities by implementing hot wire anemometry (HWA) measurement technique (Taha 2017). Each heating intensity in the dual-channel circulation loop facility for the riser channel is represented by air volumetric flow rate that is forced to flow through this developed convergent channel. In other words, naturally driven flow inside the dual-channel facility for the riser channel was mimicked by controlling forced flow through the convergent channel. Afterward, the convergent channel dimensions were calculated by using the previously reported air gas mean velocities and controlled volumetric flow rates. Table 1 shows actual velocities of the air as a coolant within the riser channel of the dual-channel circulation loop (from HWA measurements), and the mimicked one through the developed convergent channel (cold flow conditions). It is worth mention that the values of average velocity in the convergent channel is achieved by adjusting the input volumetric air flow rate to the test section and that was a big challenge for such study. Figure 1 shows a schematic diagram of the convergent channel that is used for current experiments. The convergent channel is divided into three regions: A) lower mixing region (lower plenum) which will be modeled as ideal continuous stirred tank reactor

**Table 1.** Values of the air velocity within the riser channel of the dual-channel facility and the convergent channel (separate-effect test section)

Heating intensity (W/m <sup>2</sup> )	Non-dimensional length (Z/L)	Velocity (m/s) in the dual-channel facility (hot flow system)	Velocity (m/s) in the convergent channel – separate effect test section (cold flow system)
200	0.178	0.72	0.75
	0.436	1.03	1.04
	0.546	1.09	1.10
	0.729	1.16	1.17
	0.867	1.31	1.33
600	0.178	1.37	1.25
	0.436	1.66	1.73
	0.546	1.77	1.84
	0.729	1.79	1.95
	0.867	1.86	2.22
1000	0.178	1.65	1.50
	0.436	2.26	2.08
	0.546	2.37	2.21
	0.729	2.42	2.35
	0.867	2.17	2.67
1400	0.178	1.82	1.75
	0.436	2.34	2.42
	0.546	2.57	2.57
	0.729	2.70	2.74
	0.867	2.29	3.11

(CSTR) to provide the inlet tracer concentration to the one-dimensional axial dispersion model (1D-ADM) as explained in the next sections, (B) upper mixing region (upper plenum) which is designed and developed for mimicking channel end effects (Said et al. 2017, Said et al. 2018a, Said et al. 2018b) as well as uniform sampling, and (C) core channel which mimics the riser channel without end effects. Stainless steel wire sponge has been used

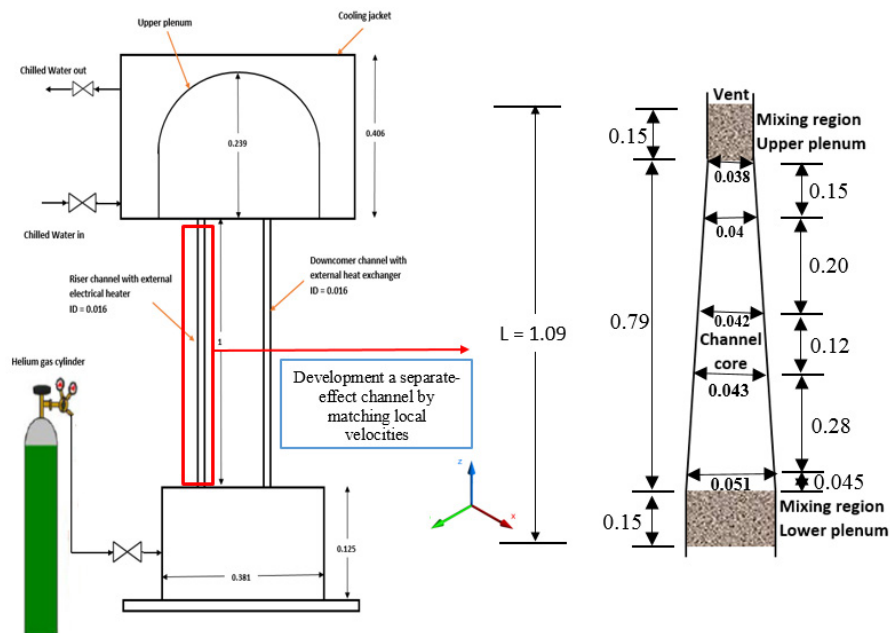


**Figure 1.** Schematic diagram for the separate effects convergent channel with a reference to the dual channel circulation loop (all dimensions in SI units: meter)

as a mixing material in the upper and lower plena. Preliminary experiments were performed to check the uniformity of mixing in the lower and upper plena (A&B). The sampling of the gas tracer was executed at different radial positions as:  $r/R = 0.0$  (center of the convergent channel),  $r/R = 0.5$ , and  $r/R = 1.0$  (near the wall surface of the convergent channel). Figure 2 shows that there were no significant differences in the measured signals of the gas tracer under the same operating conditions. This finding confirms that well-mixed conditions were achieved through lower and upper plena (A&B).

### Gaseous tracer technique

The gaseous tracer (GT) is an advanced technique used to accurately measure the residence time distribution (RTD) in a complex flow structure of single and multiphase flow systems by injecting pulse or step change gas tracer and then monitoring its concentration at the exit (Han and Al-Dahhan 2005, Han 2007, Abdulmohsin and Al-Dahhan 2016, Han et al. 2018). The measured RTD can be utilized to characterize and quantify the gas dispersion (which includes the contribution of both molecular diffusion and turbulent mixing) and identify the degree of mixing in the system. The well-designed gaseous tracer measurement technique that was developed by (Han 2007) in conjunction with the needed methodology of integral convolution to obtain a direct measurement of the gas dispersion through the test channel has been adopted in the current work. Schematic diagram and physical picture of the gaseous tracer technique configuration with the current convergent channel are shown in Figures 3 and 4, respectively. As shown in Figures 3 and 4, the gaseous tracer unit consists of a gas analyzer, gas vacuum pump, and PC with data acquisition system (DAQ). The gas analyzer is a GOW-MAC 20 series binary analyzer which contains a flowing reference thermal conductivity detector (TCD), held at room temperature. A GOW-MAC 59-300 vacuum pump was used to draw the gas sample out of the test channel and pass to the TCD. The outlet of the convergent channel is connected to the sample line of the TCD,

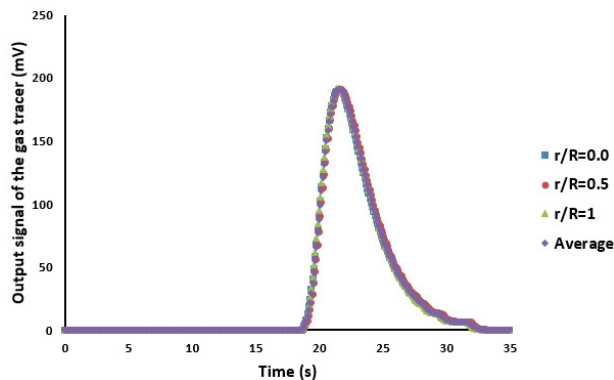


**Figure 2.** Residence time distribution (RTD) of the upper plenum for different sampling radial positions at volumetric air flow rate of 0.0034 m<sup>3</sup>/s for measurement-1 (I1-S)

where the outlet pulse response is recorded. The response from the TCD was amplified, converted to digital signals, and recorded as time series data at a sampling frequency of 10 Hz that can be adjusted as well. Common difficulties involved in the gaseous tracer technique are non-ideal injections and extra dispersion in the sampling and analysis system, which may cause significant measurement errors if they are not accounted. Due to the extra dispersion caused by the sampling and analytical components, responses measured by the gas analyzer do not exactly represent the actual tracer response. To take account of the extra dispersion effects in the sampling and analytical system, a convolution or deconvolution method needs to be applied (Levenspiel 1972). These two methods both yield a fair comparison between experimental measure-

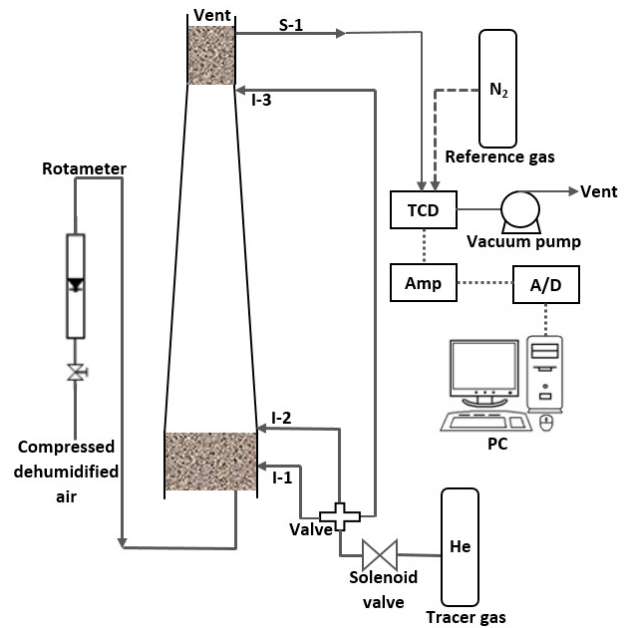


**Figure 3.** Schematic diagram of the convergent channel in conjunction with gaseous tracer technique

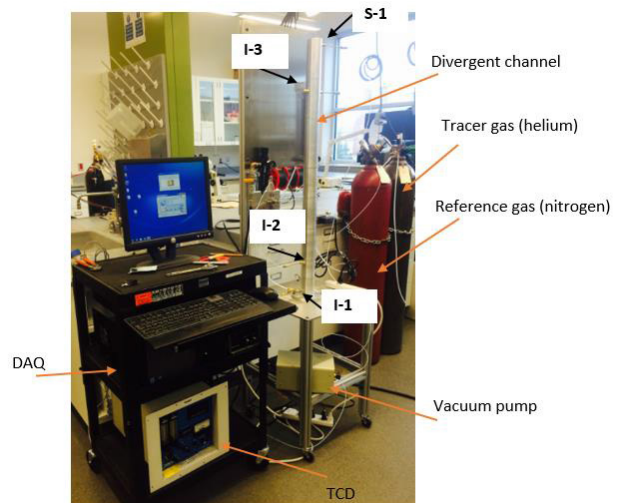


**Figure 4.** Physical picture for the convergent channel in conjunction with gaseous tracer technique

ments and reactor model predictions, either by adding the extra dispersion to the model predictions (convolution) or by removing the extra dispersion from the measurements of the whole system (deconvolution). However, due to its numerical instability, the deconvolution method is difficult to apply and is not widely used in chemical engineering research (Mills and Duduković 1989). On the other hand, the convolution method had not been employed in gas dispersion studies till 1990 (Wachi and Nojima 1990, Shetty et al. 1992, Kantak et al. 1995). Before that, the systems were assumed to have ideal tracer input and an ideal sampling and analytical system, which are not the actual cases. In the current study, the convolution integral method is implemented to quantify the extra dispersion in the lower and upper plena along with the extra dispersion exists because of the sampling and analytical system. To estimate the extra dispersion in the lower and upper plena as well as the sampling and analytical system, three ports for injection (I-1, I-2, and I-3) and one port for sampling (S-1) were designed and developed along the convergent channel as shown in Figures 3 and 4. The gas tracer (helium) introduced through a solenoid valve controlled by a digital timer, the injecting time was set to be 0.5 s as one shot, and the pulses were precisely started at the set time. Gas samples were continuously withdrawn to the gas analyzer through thin nylon tubes (1.6 mm inner diameter) under vacuum generated by the pump connected to the exit of the analytical instrument. Using the designed injection and sampling ports, for each air volumetric flow rate conditions, three measurements were obtained as shown in Table 2.

## Analysis and processing of the gas tracer signals

In this study, averaged resident time results were obtained from three replications of each experimental. Figure 5 shows a sample of the measured output signals for three experimental runs for an average volumetric flow rate of 0.0032 m<sup>3</sup>/s for measurement-1 (I1-S). It is worth mentioning that the reproducibility of all the current measurements was within  $\pm 1.5\%$ . The measured signals for all experimental tests in terms of helium concentration (mV) are normalized by the minimum ( $C_{min}$ ) and maximum ( $C_{max}$ ) concentration values to achieve a common scale for all signals from zero to one. It is worthwhile to mention here that normalizing of the output tracer signal is an important step for qualitative comparison for the

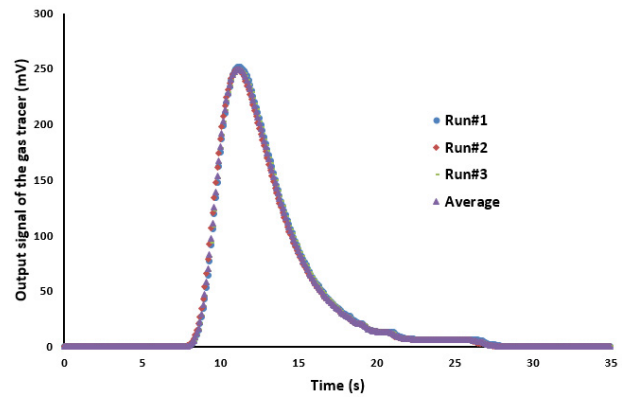


**Figure 5.** Raw signals for the three experimental runs for average volumetric air flow rate of 0.0032 m<sup>3</sup>/s for measurement of I1-S

dispersion of different sections signals within the system. The normalized value of the output tracer signal in terms of dimensionless response ( $C_{normal}$ ) can be estimated as follows (Han 2007, Abdulmohsin and Al-Dahhan 2016):

$$C_{normal} = (C_i - C_{min}) / (C_{max} - C_{min}) \quad (1)$$

For all measurements, minimum values for output tracer signals are zero as shown in Figure 5. Hence, we can rewrite Equation 1 to become as follows:

$$C_{normal} = C_i / C_{max} \quad (2)$$

Figure 6 shows normalized signals for the gas tracer under different injection positions corresponding to Table 2. It is remarkable that there is no significant difference between measurement-1 (I1-S) and measurement-2 (I2-S). Table 3 shows the mean residence time ( $t_m$ ) as a first moment of the RTD and variance ( $\sigma^2$ ) as a second moment of the RTD for the three measurements (I1-S, I2-S, and I3-S) for selected operating conditions (0.0032 m<sup>3</sup>/s and 0.0034 m<sup>3</sup>/s) just for illustration. The mean residence time ( $t_m$ ) and the variance ( $\sigma^2$ ) are defined as follows:

### Mean residence time ( $t_m$ )

It is the average value of the response time ( $t$ ), or it is the mean age of the gas tracer within the test section. Mean is the first moment of the RTD function. The mean ( $t_m$ ) is given by (Levenspiel 1972):

$$\sigma^2 = \frac{\int_0^\infty t_i c_i dt}{\int_0^\infty c_i dt} \quad (3)$$

**Table 2.** The designed three measurements for the gaseous tracer technique

Measurement	Tracer injection	Tracer detection	Tracer signal	Dispersion zones
Measurement-1 (I1-S)	I1	S	C (1)	Sampling lines+ measurement system + lower plenum + test section + upper plenum
Measurement-2 (I2-S)	I2	S	C (2)	Sampling lines + measurement system + test section + upper plenum
Measurement-3 (I3-S)	I3	S	C (3)	Sampling lines + measurement system + upper plenum

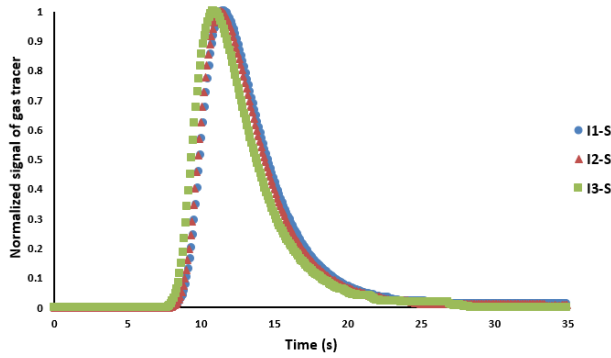


**Figure 6.** Residence time distribution (RTD) of the gas tracer for the three different measurements at average volumetric air flow rate of  $0.0015 \text{ m}^3/\text{s}$

**Table 3.** Mean residence time ( $t_m$ ) and variance ( $\sigma^2$ ) for the three measurements (I1-S, I2-S, and I3-S) for selected two volumetric air flowrates

Volumetric air flow rate: $0.0032 \text{ m}^3/\text{s}$ (corresponding to heat flux of $1000 \text{ W}/\text{m}^2$ )		
Measurement	Mean Residence time ( $t_m$ ), s	Variance ( $\sigma^2$ ), $\text{s}^2$
Measurement-1 (I1-S)	13.06	9.95
Measurement-2 (I2-S)	12.81	8.81
Measurement-3 (I3-S)	12.505	8.02
Volumetric air flow rate: $0.0034 \text{ m}^3/\text{s}$ (corresponding to heat flux of $1400 \text{ W}/\text{m}^2$ )		
Measurement	Mean Residence time ( $t_m$ ), s	Variance ( $\sigma^2$ ), $\text{s}^2$
Measurement-1 (I1-S)	12.87	8.08
Measurement-2 (I2-S)	12.77	8.42
Measurement-3 (I3-S)	12.43	7.478

or we can rewrite it in a discrete form as follows:

$$t_m = \frac{\sum t_i c_i}{\sum c_i} \quad (4)$$

### Variance ( $\sigma^2$ )

It is a measure of the gas tracer response about the mean ( $t_m$ ) and has units of ( $\text{s}^2$ ). The magnitude of the variance depends on the degree of the dispersion within the system, the greater value of variance, the higher degree of dispersion in the system and hence, the more response curve spreads and vice versa. The variance is given by the following equation (Levenspiel 1972):

$$\sigma^2 = \frac{\int_0^\infty t_i^2 c_i dt}{\int_0^\infty c_i dt} - t_m^2 \quad (5)$$

or we can rewrite it in a discrete form

$$\sigma^2 = \frac{\sum t_i^2 c_i}{\sum c_i} - t_m^2 \quad (6)$$

Variance and mean residence time results confirm that as the volumetric air flow rate (heating intensity) increases, the mean residence time and variance decrease. In other words, there is a reduction in the response curve

spreads which is achieved by increasing the volumetric air velocity and consequently the heating intensity. Also, it is clear from Table 3 that the mean residence time for measurement I1-S is greater than I2-S and I3-S as it represents the whole system, including sampling lines, lower and upper plena, measurement system, lower plenum, and test section, while the other measurements represent part of the system as shown in Table 2.

## Convolution and regression methods

The main objective of integral convolution and regression methods is to properly extract the response or residence time distribution (RTD) of the test section separately from the whole system, which includes sampling lines from the system to the thermal conductivity detector (TCD) as well as external volumes of upper and lower plena. The upper and lower plena were assumed to follow an ideal continuous stirred tank reactor (CSTR) model, while the deviation of the flow of the gas phase (coolant) from plug flow characteristics in the flow channels of prismatic block reactor is described using one-dimensional axial dispersion model (ADM) where such representation is valid if there is not much deviation from ideal plug-flow reactor (PFR) model. It is worth mentioning that these assumptions were validated by the experimentally measured signals of the gas tracer as shown in the next sections.

### Description of the gas dispersion and mixing within the lower plenum using a CSTR model

An ideal CSTR model was used to assess the gas tracer mixing within the lower plenum to get the input gas tracer concentration ( $c_m$ ) to the one-dimensional axial dispersion model (1D-ADM). Figure 7 shows the sequence of the integral convolution and regression to obtain the CSTR parameter ( $\tau_c$ ) in conjunction with the input concentration ( $c_m$ ) to the 1D-ADM. For the ideal CSTR model the concentration of the gas tracer throughout the reactor is identical to the concentration in the effluent stream, in which the CSTR model assumes perfect mixing. A non-reactive mass balance on the gas tracer for pulse injection at time  $t = 0$  into the ideal CSTR model gives for time greater than zero ( $t > 0$ ) (Levenspiel 1972, Fogler 1999, Abdulmohsin and Al-Dahhan 2016)

$$\text{Gas tracer in} - \text{Gas tracer out} = \text{Accumulation} \quad (7)$$

$$0.0 - C_i V^\circ = V (dC_i/dt) \quad (8)$$

By separating the variables and integration with  $C_i = C_{max}$  at  $t = 0$  and normalizing the concentration yields

$$C_i = C_{max} e^{-\frac{t}{\tau_c}} \quad (9)$$

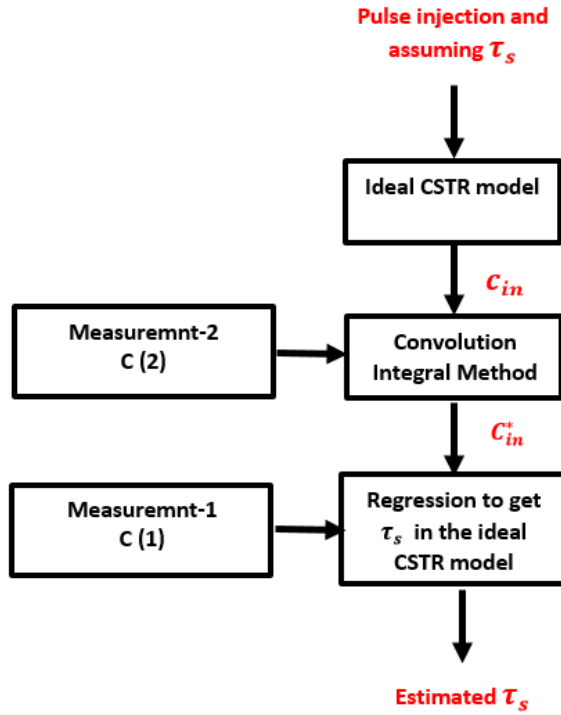


**Figure 7.** Diagram of the convolution and regression (model fit) of the tracer responses curves to get the CSTR parameter ( $\tau_s$ ) and the inlet concentration to the ADM ( $c_{in}$ )

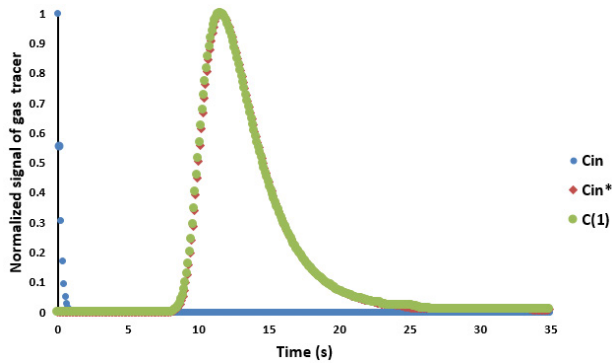


**Figure 8.** Responses of the normalized gas tracer signal for the lower plenum with CSTR model fit for 0.0015 m<sup>3</sup>/s

$$C_{in} = \frac{c_i}{C_{max}} = e^{-\frac{t}{\tau_s}} \quad (10)$$

where  $C_{in}$  is a dimensionless form for the theoretical lower plenum tracer output signal, which is the input to the 1D-ADM for the test section,  $t$  is the instant time, and  $\tau_s$  is the residence time within the lower plenum for the CSTR model. It is worth mentioning that the  $\tau_s$  of the CSTR model was estimated by the regression analysis using the measured gas tracer signal in terms of residence time distribution at the lower plenum outlet. Measurement-2 (I2-S) “C(2)” was used as the same input to the lower plenum to convolute the lower plenum as an ideal CSTR to predict the input tracer concentration ( $C_{in}^*(t)$ ) to the 1D-ADM (Levenspiel 1972, Han 2007, Abdulmohsin and Al-Dahhan 2016)

$$C_{in}^*(t) = \int_0^t C_{in}(t') \cdot C(2)(t - t') dt' \quad (11)$$

More details regarding the convolution method can be found elsewhere (Levenspiel 1972, Han 2007, Abdulmohsin and Al-Dahhan 2016). The convoluted output,  $C_{in}^*(t)$ , of the ideal CSTR prediction was compared with the measured response of the measurement-1 (I1-S) “C(1)”. Then, the parameter  $\tau_s$  was estimated by minimizing the averaged squared error between the convoluted prediction from CSTR ideal model ( $C_{in}^*(t)$ ) and the experimental measured value  $C(1)$  from measurement-1 (I1-S) as follows: (Han 2007, Abdulmohsin and Al-Dahhan 2016):

$$Error = \frac{1}{n} \sum_{j=1}^n [C_{in}^*(t_j) - C(1)(t_j)]^2 \quad (12)$$

Figures 9-11 show a good agreement between the predicted  $C_{in}^*(t)$  and measured values from experiment-1 “C(1)”, in which the average squared errors were found between  $1.2 \times 10^{-3}$  and  $4.7 \times 10^{-3}$  for volumetric air flowrate ranging from 0.0015 to 0.0034 m<sup>3</sup>/s. This indicates that the gas mixing within the lower plenum can be modeled as an ideal CSTR model for all experimental conditions. Thus, the calculated  $C_{in}$  from the ideal CSTR model in the lower plenum in conjunction with the fitted parameter  $\tau_s$  was used as an input tracer concentration to the test section, in which the 1D-ADM is based on a known input tracer concentration.

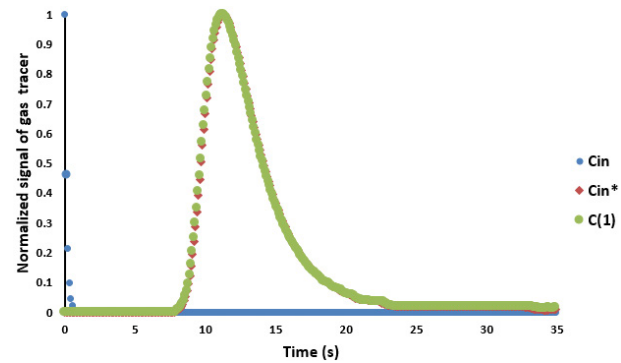


**Figure 9.** Responses of the normalized gas tracer signal for the lower plenum with CSTR model fit for 0.0024 m<sup>3</sup>/s

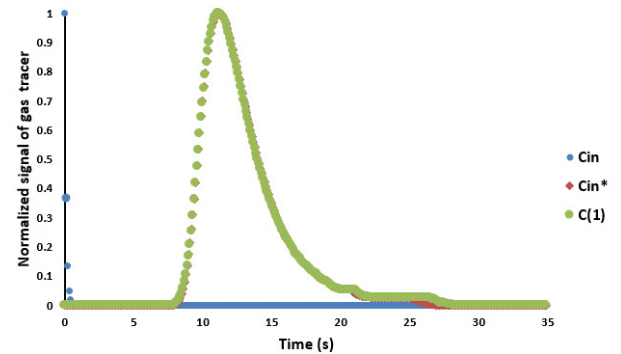


**Figure 10.** Responses of the normalized gas tracer signal for the lower plenum with CSTR model fit for 0.0032 m<sup>3</sup>/s

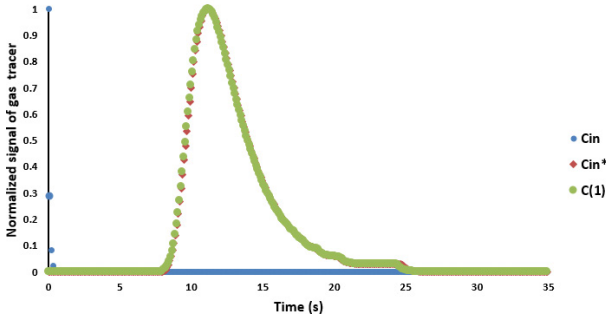


**Figure 11.** Responses of the normalized gas tracer signal for the lower plenum with CSTR model fit for 0.0034 m<sup>3</sup>/s

### Estimation of the gas dispersion within the test section using the axial dispersion model

The one-dimensional axial dispersion model (1D-ADM) is used to describe the gas tracer dispersion within the test section. In this model, there is an axial dispersion of the gas tracer, which is governed by analogy to Fick's law of diffusion. Every element of the system is transported by molecular and convective diffusions at a rate equal to " $D \cdot A(dC/dZ)$ " in conjunction with bulk flow " $UAC$ ". Where  $D$  is the effective dispersion coefficient within the system (m<sup>2</sup>/s),  $A$  is the cross sectional area (m<sup>2</sup>),  $U$  is the superficial velocity (m/s), and  $dC/dZ$  is the concentration gradient of the tracer (mole/m<sup>4</sup>). A non-reactive mole balance on the gas tracer over a short length  $\Delta Z$  of the test section in absence of radial variations yields (Levenspiel 1972, Han 2007, Abdulmohsin and Al-Dahhan 2016)

$$D \frac{\partial^2 c}{\partial z^2} - U \frac{\partial c}{\partial z} = \frac{\partial c}{\partial t} \quad (13)$$

The gas tracer concentration in the mole balance equation (Equation 13) can be rewritten in a dimensionless form as follows:

$$D \frac{\partial^2 c_{out}}{\partial z^2} - U \frac{\partial c_{out}}{\partial z} = \frac{\partial c_{out}}{\partial t} \quad (14)$$

where,

$$c_{out} = \frac{c}{c_{max}} \quad (15)$$

Once initial and boundary conditions defined, the solution of Equation 14 will yield the effluent tracer concentration ( $C_{out}$ ).

Closed-closed Danckwerts boundary conditions (Danckwerts 1953) were used in this study. An assumption is established for no radial variations of the tracer concentration or dispersion either downstream ( $Z = 0.0$ ) or upstream ( $Z = L$ ) of the test section. However, between the downstream and upstream we have axial dispersion. The corresponding boundary conditions are as follows:

At  $Z = 0.0$  (downstream)

$$U C - D \frac{dC}{dZ} = U C_{in} \quad (16)$$

The tracer concentration within Equation 16 can be rewritten in a dimensionless form as follow:

$$U C_{out} - D \frac{dC_{out}}{dZ} = U C_{input} \quad (17)$$

where,

$$C_{out} = \frac{c}{c_{max}} \quad (18)$$

$$C_{in} = \frac{c_{input}}{c_{max}} \quad (19)$$

At  $Z = L$  (upstream)

$$C_{in} = \frac{c_{input}}{c_{max}} \quad (20)$$

where  $C_{in}$  is estimated by Equation 10 with the fitted parameter of  $\tau_s$  as shown in Figure 7. The initial condition is given by

$$t = 0.0, C = 0.0 \quad (21)$$

Figure 12 shows the sequence of the integral convolution and regression analysis schematically to obtain the parameter " $D$ " of the 1D-ADM. Using  $C_{in}$  from Equation 10 as the input tracer concentration to 1D-ADM to yield an output profile  $C_{out}$ , which is then convoluted by  $C(3)$  from measurement-3 (Table 2) (Levenspiel 1972) to produce the convoluted prediction ( $C_{out}^*$ )

$$C_{out}^*(t) = \int_0^t C_{out}(t') \cdot C(3)(t - t') \cdot dt' \quad (22)$$

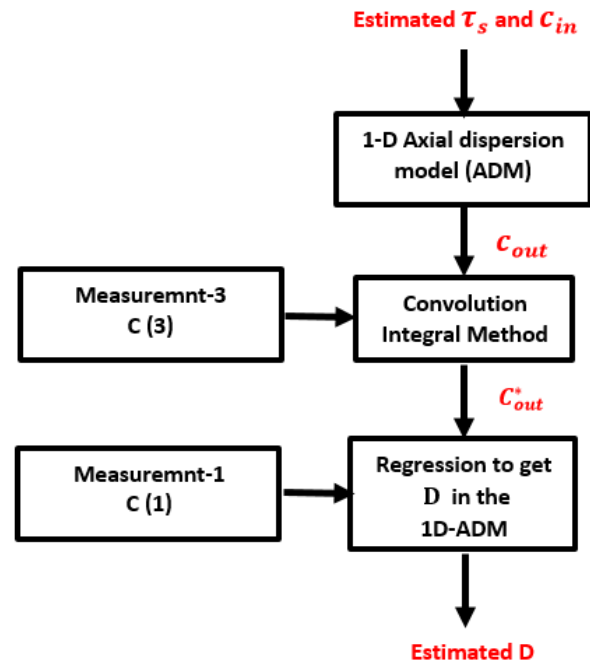


**Figure 12.** Diagram of the convolution and regression (model fits) for the gas tracer responses curves to get the dispersion coefficient ( $D$ ) for the core channel

Then the convoluted 1D-ADM prediction,  $C_{out}^*$ , was compared against the measured response of the measurement-1 “C(1)” of the whole system. Then, the dispersion coefficient parameter, D, was estimated by minimizing the averaged squared error between the convoluted prediction from 1D-ADM ( $C_{out}^*(t)$ ) and the experimental measured value  $C(1)$  from measurement-1 as follows (Levenspiel 1972, Han 2007, Abdulmohsin and Al-Dahhan 2016):

$$\text{Error} = \frac{1}{n} \sum_{j=1}^n [C_{OUT}^*(t_j) - C(1)(t_j)]^2 \quad (23)$$

Figures 13–16 show a good model fit of  $C_{out}^*$  and C(1) for selected operating conditions. The averaged squared error calculated by Equation (23) was in the range of  $6.810^{-3} \sim 22.24 \times 10^{-3}$ .

The axial dispersion coefficient (D) is used to determine the dispersive Peclet number ( $N_{pe}$ ) which represents the ratio of the rate of transport by convection to the rate of transport by dispersion as follows:

$$N_{pe} = \frac{v d}{D} \quad (24)$$

The value of  $N_{pe}$  is used to quantify the degree to which the axial dispersion affects the performance of the separate-effect test section. A high value of the  $N_{pe}$  corresponds to a slightly dispersed system.

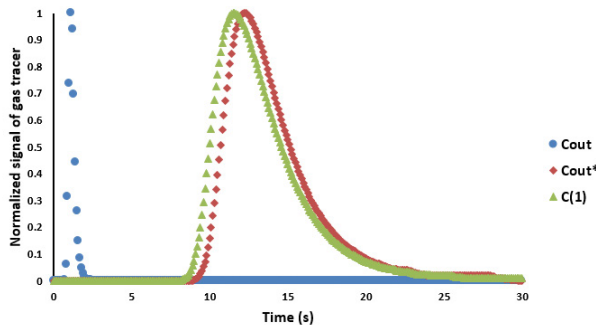


Figure 13. Responses of the normalized gas tracer signal for the core channel outlet with 1D-ADM fit for 0.0015 m<sup>3</sup>/s

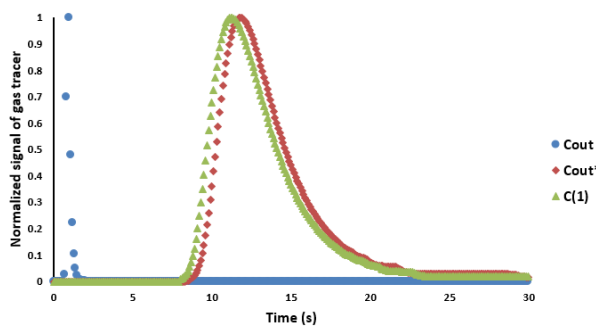


Figure 14. Responses of the normalized gas tracer signal for the core channel outlet with 1D-ADM fit for 0.0024 m<sup>3</sup>/s

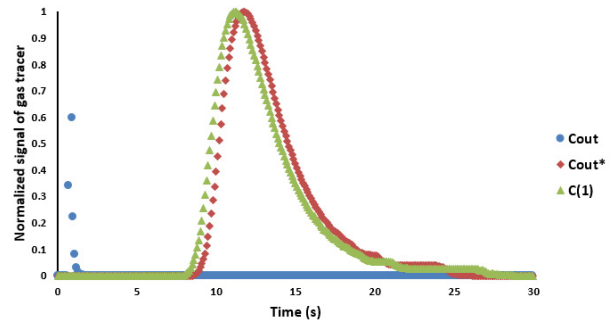


Figure 15. Responses of the normalized gas tracer signal for the core channel outlet with 1D-ADM fit for 0.0032 m<sup>3</sup>/s

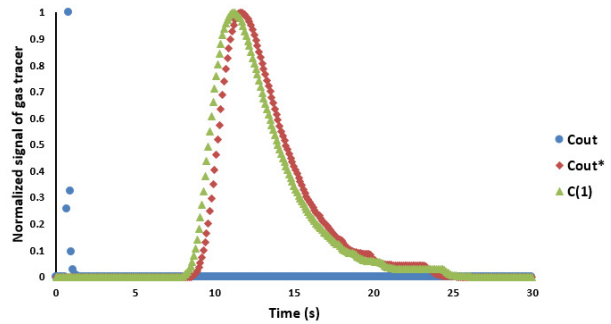


Figure 16. Responses of the normalized gas tracer signal for the core channel outlet with 1D-ADM fit for 0.0034 m<sup>3</sup>/s

**Effect of the volumetric air flow rate (corresponding to heating intensity) on the gas phase axial dispersion coefficient (D) along the riser channel**

The qualitative effect of the volumetric air flow rate on the axial dispersion coefficient (D) can be illustrated by noting that, as the dispersion coefficient (D) varies from 0 to  $\infty$ , the system behavior changes from ideal plug flow to perfect mixing. As shown in Figure 17, D values decrease with increasing the volumetric air flow rate (increasing heating intensity). This behavior can be explained by the classical approach of turbulent mass transfer (Wen and Fan 1975). The reduction in the values of axial dispersion coefficient (D) was evidently influenced by increasing the value of the eddy diffusivity of mass as turbulence was

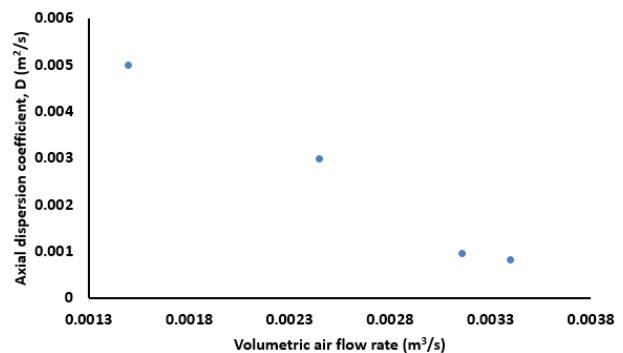
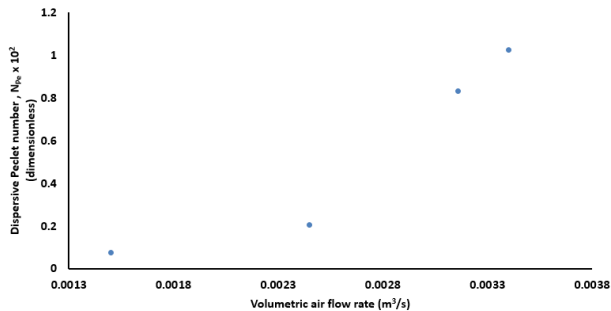


Figure 17. Effect of the volumetric air flow rate (heating intensity) on the gas phase axial dispersion coefficient (D)

generated. A similar effect has been reported by Taylor (1954), Keyes (1955), and Aris (1956) for empty tube under turbulent conditions. Besides, the Peclet number ( $N_{pe}$ ) was calculated and shown in Figure 18. The values of  $N_{pe}$  increase apparently with increasing the volumetric air flow rate (heating intensity), indicating a reduction in the rate of dispersion (Wen and Fan 1975).



**Figure 18.** Effect of the volumetric air flow rate (heating intensity) on the gas phase Peclet number ( $N_{pe}$ )

## Remarks

Gaseous dispersion experiments were conducted, for the first time, in a mimicked cold-flow separate-effect riser channel of the prismatic modular reactor using advanced gaseous tracer technique. The current separate-effect facility was designed and developed considering measured local velocities in a previous study under same operating conditions along the riser channel of the dual-channel circulation loop at mReal (Said et al. 2017). Experiments were conducted using helium as a tracer within the air as a carrier under atmospheric conditions. The gas axial dispersion coefficient ( $D$ ) and the Peclet number ( $N_{pe}$ ) have been measured and quantified under the different volumetric air flow rates of 0.0015, 0.0024, 0.0032, and 0.0034  $m^3/s$  which are corresponding to the heating intensity of 200, 600, 1000, and 1400  $w/m^2$ , respectively. The key findings are summarized as follows:

- The dispersion and mixing in the sampling lines and analytical system are a significant source of errors in the measured residence time distribution (RTD) and consequently values of  $D$  and  $N_{pe}$ . Hence, the integral convolution method is implemented to account the extra dispersion and provide accurate gaseous dispersion measurements.
- The results confirmed that a reduction in the residence time distribution (RTD) is achieved by increasing the volumetric air velocity (increasing heating intensity).
- the RTD experiments of the current study show that Peclet number increases with the volumetric air flowrate (and consequently Reynolds number). Therefore, the high volumetric flow rate mainly has the effect of decreasing the gas axial dispersion coefficient through lowering the turbulence and eddy diffusivities
- The values of the Peclet number ( $N_{pe}$ ) are found to be increased with increasing the heating intensity (as represented by volumetric air flow rate).
- The obtained axial dispersion coefficient values can be used as needed model inputs in the mass transfer measurements of the flow coolant in the prismatic block reactor as well as pressure and heat correlations.
- The measured gas phase axial dispersion coefficients ( $D$ ) and Peclet number ( $N_{pe}$ ) of the coolant gas flow in the riser channel are useful for efficient operation and safe design of the prismatic modular reactor (PMR).

## Acknowledgment

The authors acknowledge the financial support provided by the U.S. Department of Energy-Nuclear Energy Research Initiative (DOE-NERI) Project (NEUP 13-4953 (DENE0000744)) for the 4th generation nuclear energy, which made this work possible.

## References

- Abdallah IAS (2017) Experimental study of natural convection heat transfer and gaseous dynamics from dual-channel circulation loop. PhD Thesis, Missouri University of Science and Technology.
- Abdulmohsin RS, Al-Dahhan MH (2016) Axial dispersion and mixing phenomena of the gas phase in a packed pebble-bed reactor. *Annals of Nuclear Energy* 88: 100–111. <https://doi.org/10.1016/j.anucene.2015.10.038>
- Aldridge RJ (2013) Scaling study of the depressurized conduction cooldown event in the high temperature test facility using RELAP5-3D/ATHENA.
- Al-Shahri S, Said IA, Usman S, Al-Dahhan MH (2018) Plenum-to-plenum natural convection heat transfer within a scaled-down prismatic modular reactor facility. *Thermal Science and Engineering Progress* 7: 288–301. <https://doi.org/10.1016/j.tsep.2018.06.011>
- Aris R (1956) On the dispersion of a solute in a fluid flowing through a tube. *Proceedings of the Royal Society of London A: mathematical, physical and engineering sciences*, The Royal Society.
- Castañeda JA (2014) Scaling Analysis of the OSU High Temperature Test Facility during a Pressurized Conduction Cooldown Event using RELAP5-3D. M.Sc, Oregon State University.
- Danckwerts P (1953) Continuous flow systems: distribution of residence times. *Chemical Engineering Science* 2(1): 1–13. [https://doi.org/10.1016/0009-2509\(53\)80001-1](https://doi.org/10.1016/0009-2509(53)80001-1)
- Fogler HS (1999) *Elements of chemical reaction engineering*.

- Han L (2007) Hydrodynamics, back-mixing, and mass transfer in a slurry bubble column reactor for Fischer-Tropsch alternative fuels. PhD Thesis, Washington University.
- Han L, Al-Dahhan M (2005) Axial dispersion of gas phase in slurry bubble column reactor. 2005 AIChE Annual Meeting, October.
- Han L, Said IA, Al-Dahhan MH (2018) Gas Phase Back-Mixing in a Mimicked Fischer-Tropsch Slurry Bubble Column Using an Advanced Gaseous Tracer Technique. *International Journal of Chemical Reactor Engineering*. <https://doi.org/10.1515/ijcre-2018-0039>
- Haque H, Feltes W, Brinkmann G (2006) Thermal response of a modular high temperature reactor during passive cooldown under pressurized and depressurized conditions. *Nuclear Engineering and Design* 236(5–6): 475–484. <https://doi.org/10.1016/j.nucengdes.2005.10.027>
- Kantak M, Hesketh R, Kelkar B (1995) Effect of gas and liquid properties on gas phase dispersion in bubble columns. *The Chemical Engineering Journal and The Biochemical Engineering Journal* 59(2): 91–100. [https://doi.org/10.1016/0923-0467\(94\)02922-9](https://doi.org/10.1016/0923-0467(94)02922-9)
- Keyes JJ (1955) Diffusional film characteristics in turbulent flow: Dynamic response method. *AIChE Journal* 1(3): 305–311. <https://doi.org/10.1002/aic.690010306>
- Levenspiel O (1972) *Chemical Reaction Engineering*. John Wiley & Sons.
- Mills P, Duduković M (1989) Convolution and deconvolution of nonideal tracer response data with application to three-phase packed-beds. *Computers & Chemical Engineering* 13(8): 881–898. [https://doi.org/10.1016/0098-1354\(89\)85062-8](https://doi.org/10.1016/0098-1354(89)85062-8)
- Moharam MMT (2017) Experimental Investigations of Natural Circulation in a Separate-and-Mixed Effects Test Facility Mimicking Prismatic Modular Reactor (PMR) Core. PhD, Missouri University of Science and Technology.
- Said IA, Taha MM, Usman S, Al-Dahhan MH (2018a) Effect of helium pressure on natural convection heat transfer in a prismatic dual-channel circulation loop.” *International Journal of Thermal Sciences* 124: 162–173. <https://doi.org/10.1016/j.ijthermalsci.2017.10.004>
- Said IA, Taha MM, Usman S, Al-Dahhan MH (2018b) Experimental investigation of the helium natural circulation heat transfer in two channels facility using varying riser channel heat fluxes. *Experimental Thermal and Fluid Science* 93: 195–209. <https://doi.org/10.1016/j.expthermflusci.2017.12.027>
- Said IA, Taha MM, Shoaib U, Woods BG, Al-Dahhan MH (2017) Investigation of Natural Convection Heat Transfer in a Unique Scaled-Down Dual-Channel Facility. *AIChE Journal* 63(1): 387–396. <https://doi.org/10.1002/aic.15583>
- Shetty SA, Kantak M, Kelkar B (1992) Gas-phase backmixing in bubble-column reactors. *AIChE journal* 38(7): 1013–1026. <https://doi.org/10.1002/aic.690380705>
- Simoneau J-P, Champigny J, Mays B, Lommers L (2007) Three-dimensional simulation of the coupled convective, conductive, and radiative heat transfer during decay heat removal in an HTR. *Nuclear Engineering and Design* 237(15): 1923–1937. <https://doi.org/10.1016/j.nucengdes.2007.03.010>
- Taha MM (2017) Experimental investigations of natural circulation in a separate-and-mixed effects test facility mimicking prismatic modular reactor (PMR) core. PhD, Missouri University of Science and Technology.
- Taha MM, Said IA, Usman S, Al-Dahhan MH (2018a) Buoyancy-driven air flow within plenum-to-plenum facility down-come channel. *Experimental Thermal and Fluid Science* 94: 205–214. <https://doi.org/10.1016/j.expthermflusci.2018.02.003>
- Taha MM, Said IA, Usman S, Al-Dahhan MH (2018b) Natural convection inside heated channel of a facility representing prismatic modular reactor core. *AIChE Journal*. <https://doi.org/10.1016/j.expthermflusci.2018.02.003>
- Taylor G (1954) The dispersion of matter in turbulent flow through a pipe. *Proceedings of the Royal Society of London A: Mathematical, Physical and Engineering Sciences*, The Royal Society.
- Tung Y-H, Johnson RW (2011) CFD calculations of natural circulation in a high temperature gas reactor following pressurized circulator shutdown. ASME 2011 International Mechanical Engineering Congress and Exposition, IMECE 2011. <https://doi.org/10.1115/IMECE2011-64259>
- Tung Y-H, Ferng Y-H, Johnson RW, Chieng C-C (2013) Study of natural circulation in a VHTR after a LOFA using different turbulence models. *Nuclear Engineering and Design* 263: 206–217. <https://doi.org/10.1016/j.nucengdes.2013.04.009>
- Tung Y-H, Ferng Y-H, Johnson RW, Chieng C-C (2016) Transient LOFA computations for a VHTR using one-twelfth core flow models.” *Nuclear Engineering and Design* 301: 89–100. <https://doi.org/10.1016/j.nucengdes.2016.03.002>
- Tung Y-H, Johnson RW, Ferng Y-M, Chieng C-C (2014) Modeling strategies to compute natural circulation using CFD in a VHTR after a LOFA. *Nuclear Engineering and Design* 275: 80–90. <https://doi.org/10.1016/j.nucengdes.2014.04.012>
- Wachi S, Nojima Y (1990) Gas-phase dispersion in bubble columns. *Chemical Engineering Science* 45(4): 901–905. [https://doi.org/10.1016/0009-2509\(90\)85012-3](https://doi.org/10.1016/0009-2509(90)85012-3)
- Wen C-Y, Fan L-t (1975) *Models for Flow Systems and Chemical Reactors*. M. Dekker.

## Notation

$c$	concentration of the tracer in the gas phase, mol/m <sup>3</sup>	$C_{in}^*$	dimensionless convoluted tracer concentration in the gas at the lower plenum outlet
$c_{min}$	minimum concentration of the tracer in the gas phase, mol/m <sup>3</sup>	$C_{out}$	dimensionless tracer concentration in the gas phase at the test section outlet
$c_{max}$	maximum concentration of the tracer in the gas phase, mol/m <sup>3</sup>	$C_{out}^*$	dimensionless convoluted tracer concentration in the gas at the test section outlet
$c_{inj}$	concentration of the injection tracer, mol/m <sup>3</sup>	$C_{normal}$	normalized value of the output tracer signal (dimensionless)
$C_{in}$	dimensionless tracer concentration in the gas phase at the lower plenum outlet		

---

D	effective axial dispersion coefficient of the gas phase, $\text{m}^2/\text{s}$	t	time, s
L	length of the separate-effect test section, m	$t_m$	mean residence time of the bed, s
d	inlet inside diameter of the separate effect test section, m	V	volume of the air, $\text{m}^3$
n	total number of experimental data points	$V^0$	volumetric air flow rate, $\text{m}^3/\text{s}$
$N_{pe}$	dispersive Peclet number ( $V d/D$ ), dimensionless	Z	axial distance along the test section, m
U	superficial gas velocity, (m/s)	Z/L	non-dimensional length, dimensionless
		$\sigma^2$	variance, $\text{s}^2$
		$\tau_s$	CSTR parameter, s